JACS
JOURNAL OF THE AMERICAN CHEMICAL SOCIETY
pubs.acs.org/JACS
Article

Water Dynamics in the Formation of Single-Component-Based Multiphasic Droplets

Laicheng Zhou, Liheng Lu, Yang Zhang, Jing Wang, Jianjun Cheng, and Huaimin Wang*

Cite This: https://doi.org/10.1021/jacs.5c10784
Read Online

ABSTRACT: Despite the significant presence of water in the liquid−liquid phase separation (LLPS) of biomolecular condensates, its critical role beyond the solvent effects has been largely overlooked. In this study, we investigate the synergistic effects of water on modulating the substructure and properties of biomolecular condensates. We designed and synthesized a series of peptide-based droplets with varying microstructures. Utilizing in situ Raman and Fourier transform infrared (FTIR) spectroscopy, we elucidate how an increased hydrogen bonding network between the peptide and water, coupled with a decreased hydrogen bonding network among peptides, drives the transition from multiphasic to homogeneous configurations. Furthermore, we demonstrate that this transformation can be dynamically regulated by adjusting peptide-water interactions through the application of Chaotropic and Kosmotropic agents. Our findings underscore the essential role of hydration water in the LLPS of single-component systems, paving the way for innovative strategies in the design and modulation of advanced hydrated materials.

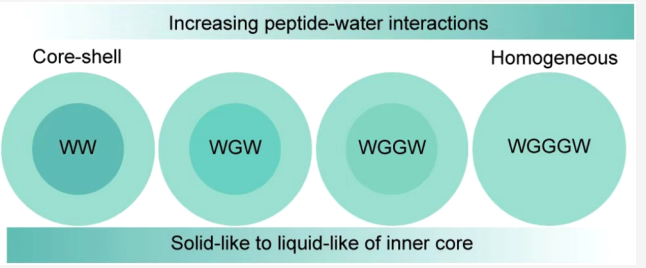

INTRODUCTION

Water is an essential component of cellular systems, playing a crucial role in maintaining osmotic balance, facilitating protein folding, and enabling molecular recognition.[1−5] Beyond these foundational roles, water significantly influences molecular self-assembly processes in supramolecular chemistry, impacting phenomena such as adhesion,[6−9] gelation,[10−13] fibrillation[14−17] and among others.[18−25] The unique tetrahedral structure of liquid water allows each water molecule to establish hydrogen bonds with four neighboring molecules, forming a dynamic three-dimensional network.[1,26,27] The introduction of solutes disrupts this equilibrium, prompting a reorganization of water molecules in their vicinity.[26] Solutes exhibit distinct effective solvated volumes based on their hydrophobic or hydrophilic properties, classified into hydration water—comprising closely associated first and second hydration shells—and bulk water, located beyond these shells.[17,27] Interactions within these systems can be categorized as solute−solvent, solute−solute, and solvent−solvent interactions, each contributing to the stabilization of the overall system.[27−29] External factors such as pH, temperature, redox status, and ionic strength can induce the release of hydration water into the bulk phase.[27,29] This entropically favorable process, coupled with enthalpically driven intermolecular interactions, could be sufficient to trigger molecular self-assembly or phase separation.[27,29] While the role of water in supramolecular chemistry is well established, its influence on liquid−liquid phase separation (LLPS) remains underexplored.[30,31] Recent studies have begun to illuminate water's role in LLPS,[27,32−35] however, the mechanisms by which water modulates the substructure of LLPS droplets are still poorly understood.

In this study, we investigated a series of short peptides, WG_nW (n = 0∼3), that undergo LLPS to form liquid droplets (Figure 1a). We discovered that dipeptide WW forms core−shell droplets with a solid-like inner core surrounded by a liquid-like outer shell. As the peptide composition shifts from WW to WGGGW, the inner core transitions from solid-like to liquid-like, resulting in homogeneous droplets (Figure 1b). Through molecular engineering and amino acid mutations, we demonstrated that the core−shell structure is primarily dictated by the amphiphilicity of the amino acid composition, rather than the peptide length or arrangement. Using in situ Raman and FTIR, we revealed a decrease in peptide−peptide interactions alongside an increase in peptide-water interactions, correlating with the transition to homogeneous droplets (Figure 1c). Molecular dynamics simulations further elucidate how the interplay between peptide−peptide and peptide-water interactions governs the substructures of these droplets. Importantly, we showed that dynamic control over transformation from core−shell condensates to homogeneous liquid droplets can be achieved by modulating peptide-water

Received: June 25, 2025
Revised: August 5, 2025
Accepted: August 6, 2025

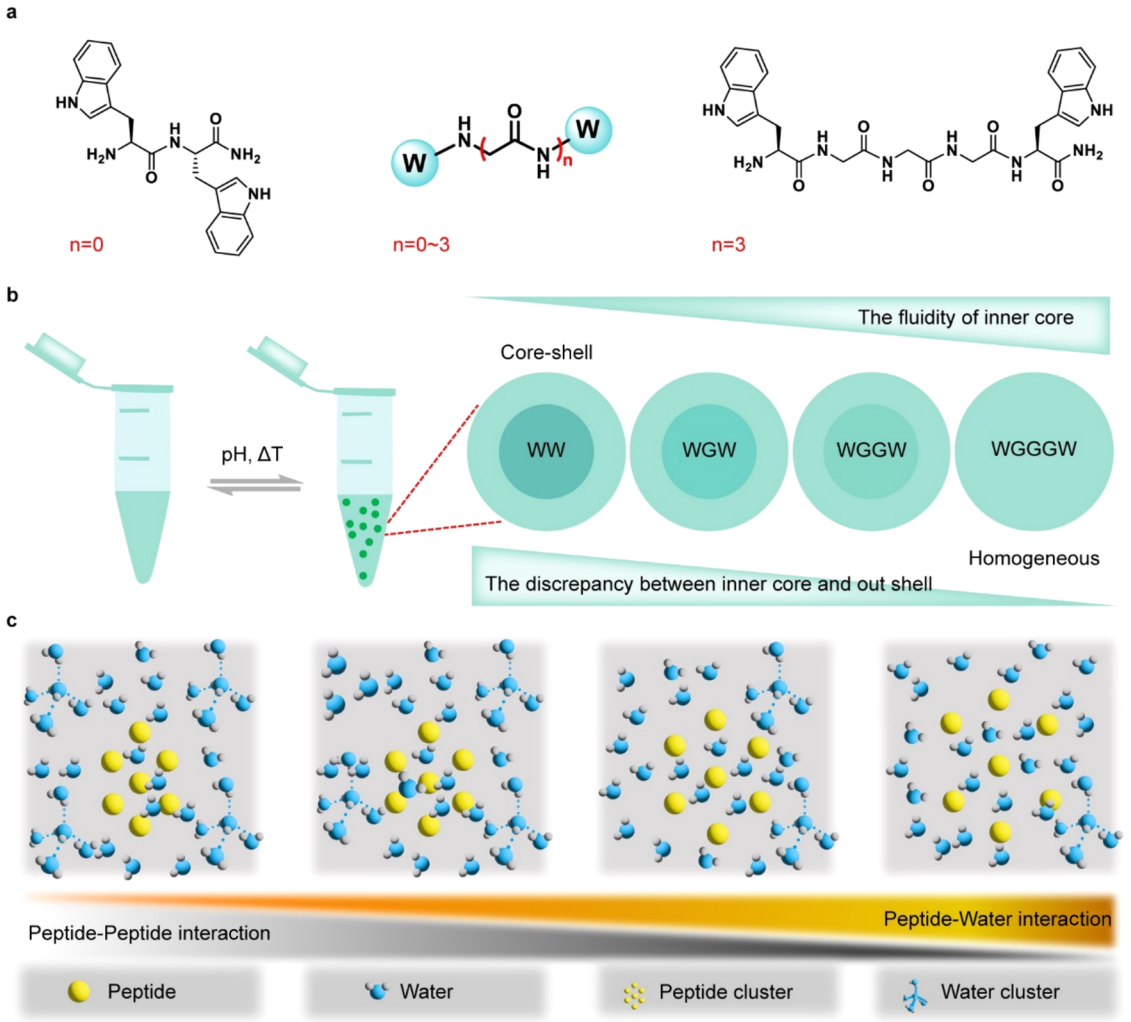

Figure 1. Liquid−liquid phase separation of peptides WG_nW (n = 0~3). (a) Molecular structure of peptides WG_nW (n = 0~3). (b) Schematic illustration of liquid−liquid phase separation of peptides WG_nW (n = 0~3). (c) Schematic illustration of the changes of peptide−peptide, peptide-water, and water−water interaction from WW to WGGGW system.

interactions using "Chaotropic" and "Kosmotropic" agents.[26] Our findings highlight the critical role of hydration water in regulating the structural dynamics of liquid droplets, offering new insights into the design and modulation of advanced hydrated materials with significant implications in biophysics and materials science.

RESULTS AND DISCUSSION

Engineering Single-Component Droplets with Varying Architectures via LLPS. Recent studies have shown that ditryptophan (WW) and its derivatives generally do not promote LLPS effectively.[36,37] However, our recent findings reveal that tryptophan modified with a C-terminal amide significantly enhances the design of short peptide-based liquid droplets.[38] This modification facilitates the formation of core−shell structure droplets, primarily due to the large aromatic ring of tryptophan, which strengthens homotypical $\pi-\pi$ interactions compared to other amino acids.[38] Notably, the distinctive Raman peaks of tryptophan serve as the marker for various noncovalent interactions, aiding in the exploration of molecular mechanisms.[39,40]

Building on these insights, we designed a series of short peptides, WG_nW (where n = 0~3), utilizing a sticker-spacer model to promote LLPS (Figure 1a). We selected varying lengths of glycine as spacers, given its high frequency and significant presence in intrinsically disordered proteins (IDPs) or intrinsically disordered regions (IDRs) associated with LLPS.[41−43] Upon exposure to external stimuli such as pH and temperature, clear peptide solutions undergo LLPS, resulting in the formation of a white milk emulsion (Figure 2a). Confocal laser scanning microscopy (CLSM) imaging confirmed the presence of spherical droplets (Figure 2b). Phase diagrams constructed from pH and concentration data reveal that all peptides remain soluble in water at pH below 6.0. However, as the pH increases to approximately 7.0, phase separation is initiated, leading to the emergence of condensed liquid droplets alongside a dilute phase (Figure 2c). This behavior suggests that the deprotonation of the N-terminal amine group likely triggers the LLPS, underscoring the intricate relationship between pH and droplet formation.[38]

To investigate the inhomogeneous nature of the droplets formed, we employed fluorescence lifetime imaging microscope (FLIM) using the polarity-sensitive fluorophore sulfonamide benzoxadiazole (SBD).[44] This technique enabled us to evaluate the average microenvironmental polarity within the droplets. In homogeneous droplets, the fluorescence

https://doi.org/10.1021/jacs.5c10784
J. Am. Chem. Soc. XXXX, XXX, XXX−XXX

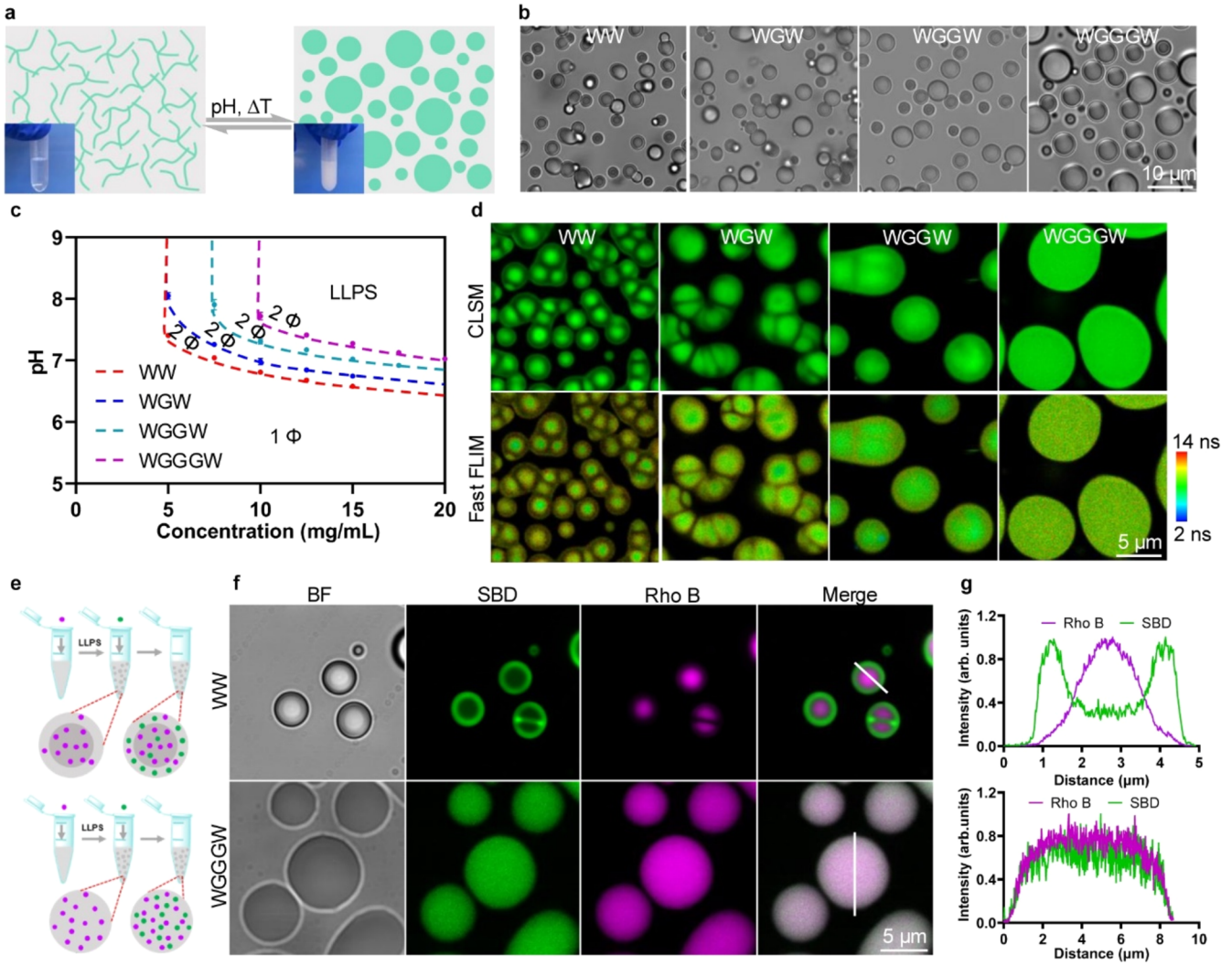

Figure 2. Core−shell condensates to homogeneous droplets formed via LLPS of WG_nW (n = 0∼3). (a) Schematic illustration of liquid droplet formation through LLPS. (b) Microscope images of the droplets formed by peptide WG_nW (n = 0∼3). (c) pH-concentration phase diagrams of peptide WG_nW (n = 0∼3). (d) Confocal and fast FLIM images of the droplets formed by peptide WG_nW (n = 0∼3). (e) Schematic illustration of the distribution of fluorophores (Rho B and SBD) added before and after the droplet's formation. (f) CLSM images of the distribution of Rho B and SBD in the droplets formed by WW and WGGGW. (g) Fluorescence intensity distribution plots at cross sections. The concentration in panels b,d is 10 mg/mL for WW, WGW, and WGGW, and 15 mg/mL for WGGGW. The pH value is 7.5 ± 0.5.

lifetime of SBD would remain constant; however, variations in the lifetime indicate microenvironmental differences. Our findings reveal that, with the exception of the peptide WGGGW, the SBD lifetime in the inner core differs significantly from that in the outer shell for all other droplets, highlighting their inhomogeneous microenvironment. Furthermore, SBD exhibits an uneven distribution with fluorescence intensity in the inner core markedly higher than in the outer shell. This discrepancy diminishes from WW to WGGGW (Figure 2d), suggesting that the structural differences between the inner core and out shell become less pronounced as the peptide composition transitions. To visualize the core−shell structure more effectively, we utilized two distinct fluorescent molecules: SBD and rhodamine B (Rho B). Rho B was introduced prior to droplet formation, and SBD was added afterward. In the core−shell droplets formed by WW, Rho B predominantly localized within the inner core, whereas SBD was primarily distributed in the outer shell (Figure 2e−g, top panel). In contrast, for the homogeneous droplets formed by WGGGW, both SBD and Rho B exhibited a uniform distribution (Figure 2e−g, bottom panel). Additionally, when two WW droplets fused, the inner core remained intact but was deformed by the merging outer shell. This observation underscores the solid-like nature of the inner core in comparison to the more fluid outer shell, further emphasizing the architectural differences within these droplets.

Transition of the Inner Core from Solid-Like to Liquid-Like States. Upon contact, two liquid-like droplets tend to fuse, resulting in a larger spherical shape.[45,46] The fusion dynamics are influenced by the ratio of surface tension to viscosity: liquid-like droplets typically exhibit faster fusion rates compared to solid-like condensate.[45] To assess the liquidity of droplets formed by WG_nW (n = 0∼3), we systematically measured the coalescence time of pairs of spherical droplets. The entire fusion process was well characterized by exponential relaxation, as evidenced by the time-course microscopy images (Figure 3a). By plotting the aspect ratio against time during fusion, we determined the characteristic relaxation time (τ) through exponential fitting[46] (Figure 3a). Our results revealed that the fusion speeds of WW

https://doi.org/10.1021/jacs.5c10784
J. Am. Chem. Soc. XXXX, XXX, XXX−XXX

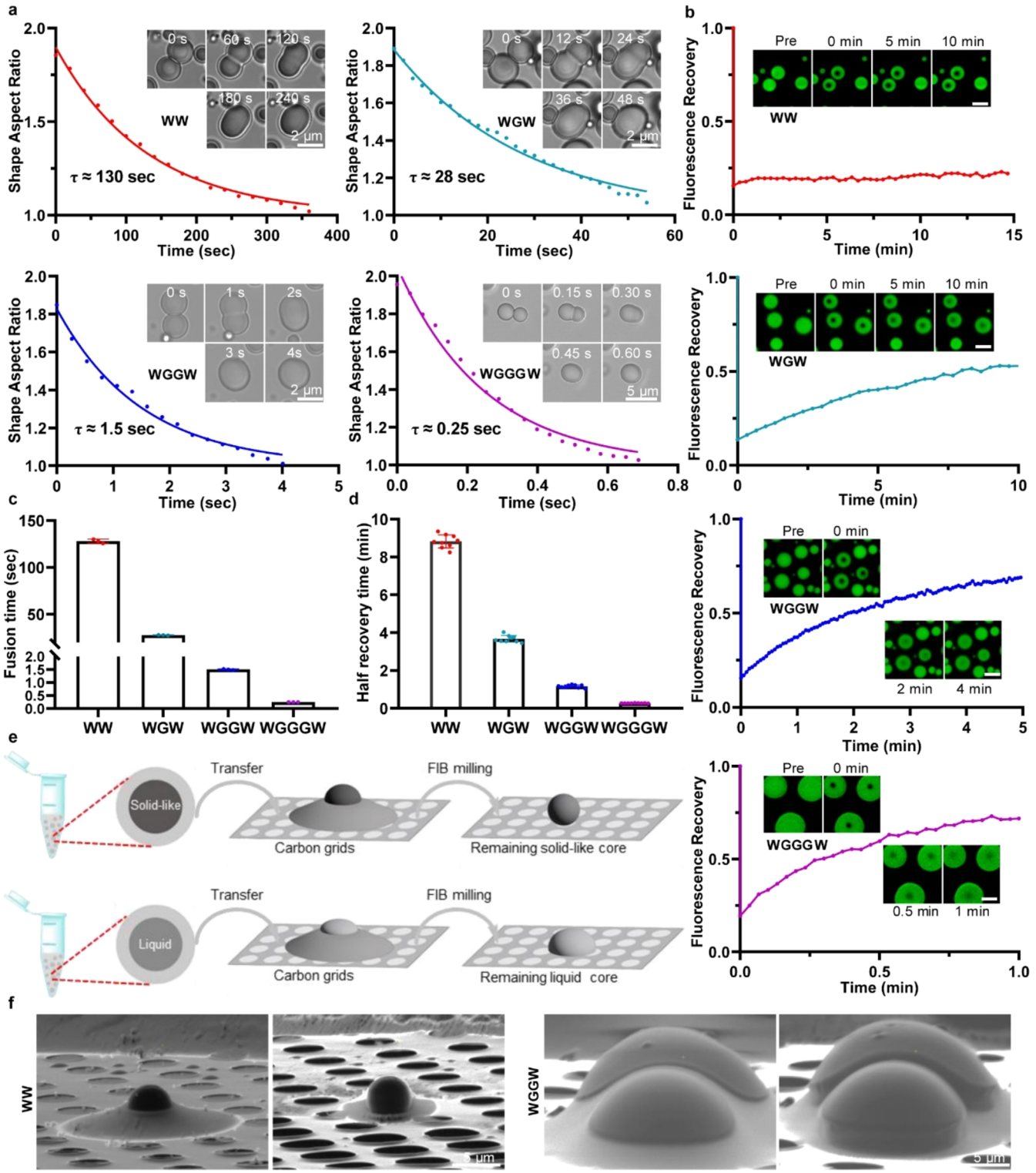

Figure 3. Solid-like inner core gradually turned to liquid-like from WW to WGGGW. (a) Time course of the distance between the two droplets formed by peptide WG_nW (n = 0~3), the fusion events are well fit by an exponential decay, which is used to determine fusion time scale τ. (b) FRAP analysis of the inner core of the droplets, (b) and representative data are shown. Scale bar: 5 μm. (c, d) Fusion time τ and Half-recovery time $\tau_{1/2}$ of the droplets formed by WG_nW (n = 0~3). (e) Schematic illustration of the changes of the condensates under gallium ion beam sputtering. (f) Cyro-FIB-SEM images of the droplets formed by WW and WGGW. For all of the experiments, the concentration of WW, WGW, and WGGW is 10 mg/mL, while WGGGW is 15 mg/mL (pH = 7.5 ± 0.5).

droplets were the slowest, while WGGGW droplets fused the fastest, indicating that WW droplets exhibit more solid-like behavior, whereas WGGGW droplets demonstrate liquid-like characteristics (Figure 3a,c). Notably, the fusion of core−shell droplets involves deformation of the inner core, which contributes to a slower fusion process. This result suggests that the liquidity of the inner core significantly affects the overall fusion speed. To further verify this hypothesis, we

https://doi.org/10.1021/jacs.5c10784
J. Am. Chem. Soc. XXXX, XXX, XXX−XXX

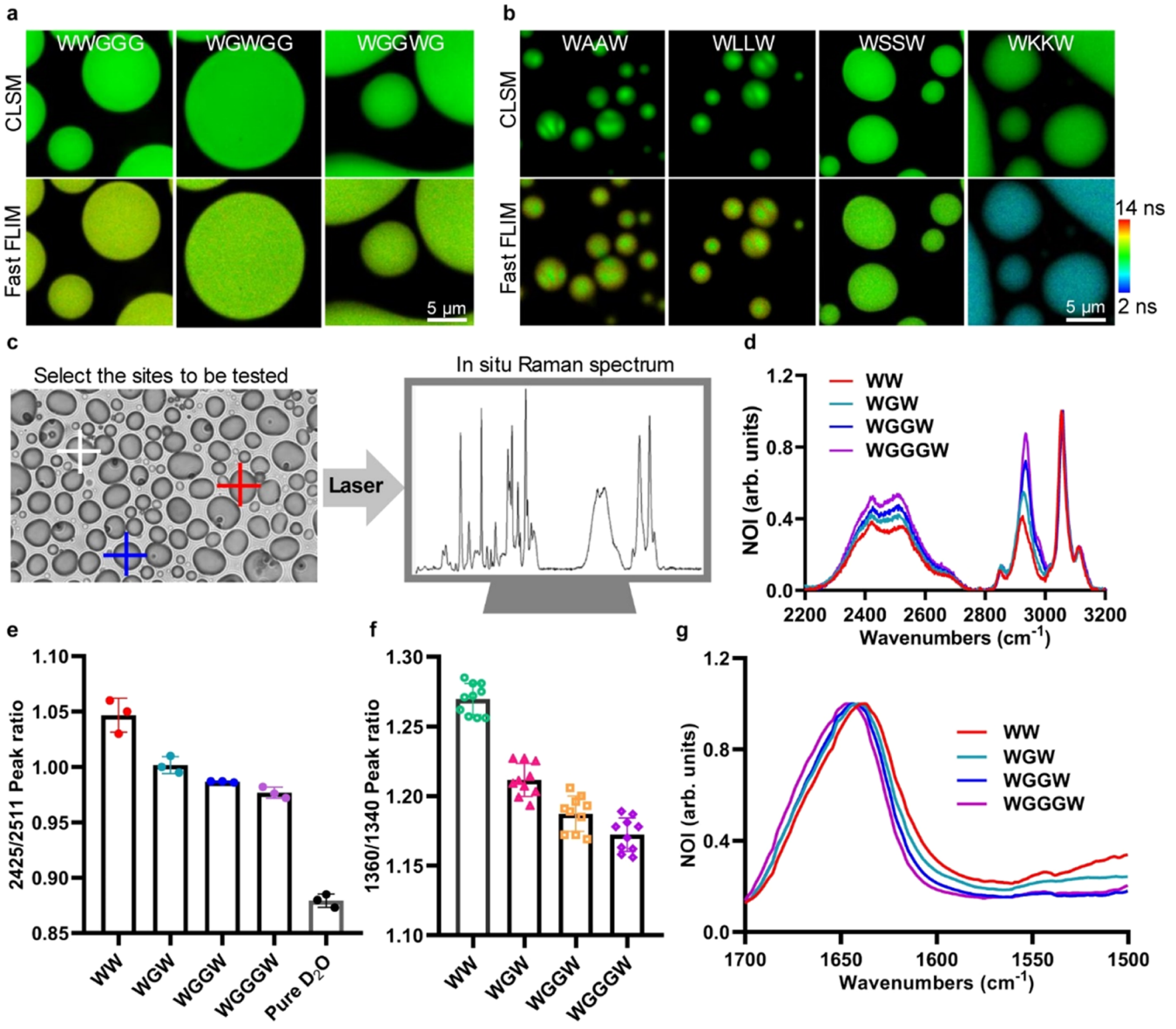

Figure 4. Mechanism underlying the transformation from core−shell condensates to homogeneous droplets. (a) Confocal and fast FLIM images of the droplets formed by WWGGG (15 mg/mL), WGWGG (15 mg/mL), WGGWG (15 mg/mL), and SBD (1 μM), (pH = 7.5 ± 0.5). (b) Confocal and fast FLIM images of the droplets formed by WAAW (5 mg/mL, pH = 7.5 ± 0.5), WLLW (2 mg/mL, pH = 7.5 ± 0.5), WSSW (20 mg/mL, pH = 7.5 ± 0.5), and WKKW (20 mg/mL, pH = 10 ± 0.5). (c) Schematic illustration of the in situ Raman spectroscopy. (d) Partial enlarged Raman spectrum of the droplets formed by peptide WG_nW (n = 0∼3) in D_2O, the relative intensity of low- and high-frequency stretch mode indicate different H−bonded networks of water. (e) I_{2425}/I_{2511} peak ratio (intensity) of the in situ Raman spectrum of the droplets formed by peptide WG_nW (n = 0∼3). (f) I_{1360}/I_{1340} peak ratio (intensity) of the in situ Raman spectrum of the droplets formed by peptide WG_nW (n = 0∼3). (g) Partial enlarged IR spectra of the droplets formed by peptide WG_nW (n = 0∼3) in D_2O.

employed fluorescence recovery after photobleaching (FRAP) to analyze the dynamics of the inner core (Figure 3b). The WW inner core exhibited approximately 20% fluorescence recovery with a half-time of around 9 min. In contrast, the homogeneous WGGGW droplets displayed rapid fluorescence recovery, with a half-time of less than 1 min (Figure 3d). The increasing rate and efficiency of fluorescence recovery from WW to WGGGW indicate a transition from a solid-like inner core to a liquid-like state, ultimately leading to the formation of homogeneous WGGGW droplets.

To further illustrate the solid-to-liquid transition of the inner core, we employed Focused Ion Beam Scanning Electron Microscopy (FIB-SEM) to compare the inner cores of WW and WGGW. Due to the higher fluidity of the outer shell, it collapses rapidly, exposing the inner core when the core−shell droplets are transferred to a copper grid. The samples are then plunge-frozen in liquid ethane and transferred to a cryo-stage maintained at −191 °C, followed by cryo-FIB milling and cryo-SEM imaging (Figure 3e). The results showed that the inner core was surrounded by the collapsed outer shell, which was subsequently removed by using gallium ion beam milling. Once the inner core was fully exposed, the inner core of WW retained a spherical structure, while the inner core of WGGW appeared collapsed (Figure 3f). This contrast underscores the greater solidity of the inner core in WW compared to the more fluid-like nature of that in WGGW.

Mechanism Underlying the Transition from Core−Shell Condensates to Homogeneous Droplets. To

https://doi.org/10.1021/jacs.5c10784
J. Am. Chem. Soc. XXXX, XXX, XXX−XXX

elucidate the mechanism behind the transition of the inner core from solid-like to liquid-like behavior, and then ultimately formed homogeneous droplets, we first examined the influence of the scattering degree of stickers by comparing the peptide WGGGW with WWGGG, WGWGG, and WGGWG. Fluorescence microscopy and fast FLIM images revealed that all these peptides form homogeneous droplets (Figure 4a). Next, we explored how the amphiphilicity of peptides affects the substructure of the droplets through targeted amino acid mutations. While the more hydrophobic peptides WAAW and WLLW formed core−shell droplets, the more hydrophilic peptides WSSW and WKKW resulted in homogeneous droplets (Figure 4b). These findings suggest that peptide-water interactions are crucial in determining the substructures of condensates. Specifically, hydrophilic amino acids enhance peptide-water interactions, whereas hydrophobic residues weaken these interactions.

To test this hypothesis, we systematically measured changes in the hydrogen bonding network among peptide−peptide, peptide-water, and water−water interactions across the WW to WGGGW systems. The strength of the hydrogen bonding network among water molecules can be reflected in its O−H stretch mode; lower stretch frequencies indicate stronger hydrogen bonds, as evidenced by ultrafast infrared, vibrational sum-frequency, and in situ Raman spectroscopy.[47−51] Using in situ Raman spectroscopy, we measured the O−D stretch mode of D_2O in the WG_nW (n = 0∼3) droplets (Figure 4c). All Raman spectra shared two broad peaks at around 2425 and 2511 cm^{-1}, differing in relative intensity. The peak at 2425 cm^{-1} corresponds to stronger hydrogen bonding among water molecules compared to the peak at 2511 cm^{-1} since lower O−D stretch frequency report on stronger hydrogen bond strength of water.[47] The relative intensity of the peaks at 2425 and 2511 cm^{-1} differs from WW to WGGGW, indicating different populations of strong and weak hydrogen-bonded water (Figure 4d). To quantitatively evaluate the relative hydrogen bond strength, we measured the peak ratio of 2425 to 2511 cm^{-1} (Figure 4e). Compared to pure D_2O, this peak ratio increased in all the droplets, indicating a strengthened hydrogen bonding network in the droplets of WG_nW (n = 0∼3). Furthermore, the peak ratio gradually decreased from WW to WGGGW, reflecting a diminished hydrogen bond network among water molecules. This trend suggests that water molecules are more easily released from their hydrogen bonding networks, allowing for stronger interactions with the peptides.

We also analyzed the Raman spectra of peptides in the droplets and quantified the intensity ratio of the peak near 1360 and 1340 cm^{-1} (I_{1360}/I_{1340}), which serves as a marker for hydrophobic interactions of the tryptophan[40] (Figure 4f). The decreasing intensity ratio from WW to WGGGW indicates that the tryptophan side chains are exposed to a less hydrophobic environment, reflecting reduced hydrophobic interactions. Additionally, we investigated the hydrogen bonding network among the peptide backbones using FTIR.[52,53] Vibrational spectroscopy can directly assess the strength of hydrogen bonds, as stronger hydrogen bonding typically lowers the frequency of stretching vibrations.[53] The FTIR spectra revealed a red shift in the amide I frequency from approximately 1650 to 1647, 1644, 1641, and 1638 cm^{-1}, respectively, for droplets transitioning from WGGGW to WW (Figure 4g). This shift demonstrates an increasing hydrogen bonding network in the droplets from WGGGW to WW.

In addition to hydrogen bonding, amide I vibration is sensitive to the secondary structure of protein or peptide backbones. The amide I band in the range of 1639−1654 cm^{-1} in D_2O typically correlates with disordered structures, while the range of 1615−1638 cm^{-1} in D_2O is characteristic of β-sheet structures.[52,53] The results indicate a growing tendency to form a β-sheet structure as we move from WGGGW to WW. This transition may explain the transformation from homogeneous droplets to core−shell droplets and the transition from a liquid-like to a solid-like inner core.

All-Atom Molecular Dynamics (MD) Simulation. To complement our experimental findings, we conducted all-atom MD simulations using the Gromacs 2022.1 software package with the Amber14sb force field.[54] Simulations were performed under a constant temperature and periodic boundary conditions. Peptide molecules were solvated in a cubic box measuring 6.0 nm × 6.0 nm × 6.0 nm, using the TIP3P water model.[55] We minimized the energy of the initial structure using the steepest descent method for 50,000 steps, followed by NPT ensemble simulations to ensure equilibrium. The Leap-Frog method was used to integrate the equations of motion, and the PME method evaluated long-range electrostatic interactions.[56] The truncation distances for van der Waals and Coulomb interactions were set at 12 Å with updates performed every 10 steps. We employed the Lincs algorithm[57] and V-rescale temperature coupler,[58] along with the Parrinello−Rahman method,[59] to constrain all bond lengths (parameters: lincs_iter = 1 and lincs_order = 4), heat the system from 0 to 298.15 K, maintain a pressure of 1 bar, and ensure pressure isotropy.

Nonbonded interactions were calculated using a twin-range neighborhood list approach, with short-range and long-range cutoff distances of 9 and 14 Å, respectively. Hydrogen bond criteria were defined as a donor−acceptor angle of less than 30° and a donor−acceptor distance of not exceeding 0.35 nm. Four simulated systems (WW, WGW, WGGW, and WGGGW) were constructed, each containing 30 peptide molecules and 2000 solvent water molecules to ensure computational efficiency while capturing key interaction trends. Although this peptide-to-water ratio is higher than that in experiments, the simulations were intended to provide qualitative insights into peptide−water and peptide−peptide interactions rather than replicate exact experimental concentrations. Initial atomic velocities were sampled from a Maxwell−Boltzmann distribution at the target temperature. The simulation was conducted for 100 ns using a 2 fs integration time step, comprising 50 million steps in total, with system coordinates saved at regular intervals to generate an ensemble of 10,000 conformations.

Trajectory analysis and visualization were performed by using the built-in analytical tools of GROMACS along with Visual Molecular Dynamics (VMD) software for structural representation. Conformational evolution of the four molecular systems was analyzed through comparative structural assessment of the initial and final states, with representative structures illustrated in Figure S1. Initially, the peptides in all four systems exhibited dispersed spatial distributions. Following 100 ns of molecular dynamics simulation, the systems demonstrated differential aggregation behavior. Notably, a clear inverse correlation was observed between the degree of peptide assembly and spacer length, with aggregation propensity diminishing as the spacer length increased. In the WW system, peptide molecules aggregated into a single

https://doi.org/10.1021/jacs.5c10784
J. Am. Chem. Soc. XXXX, XXX, XXX−XXX

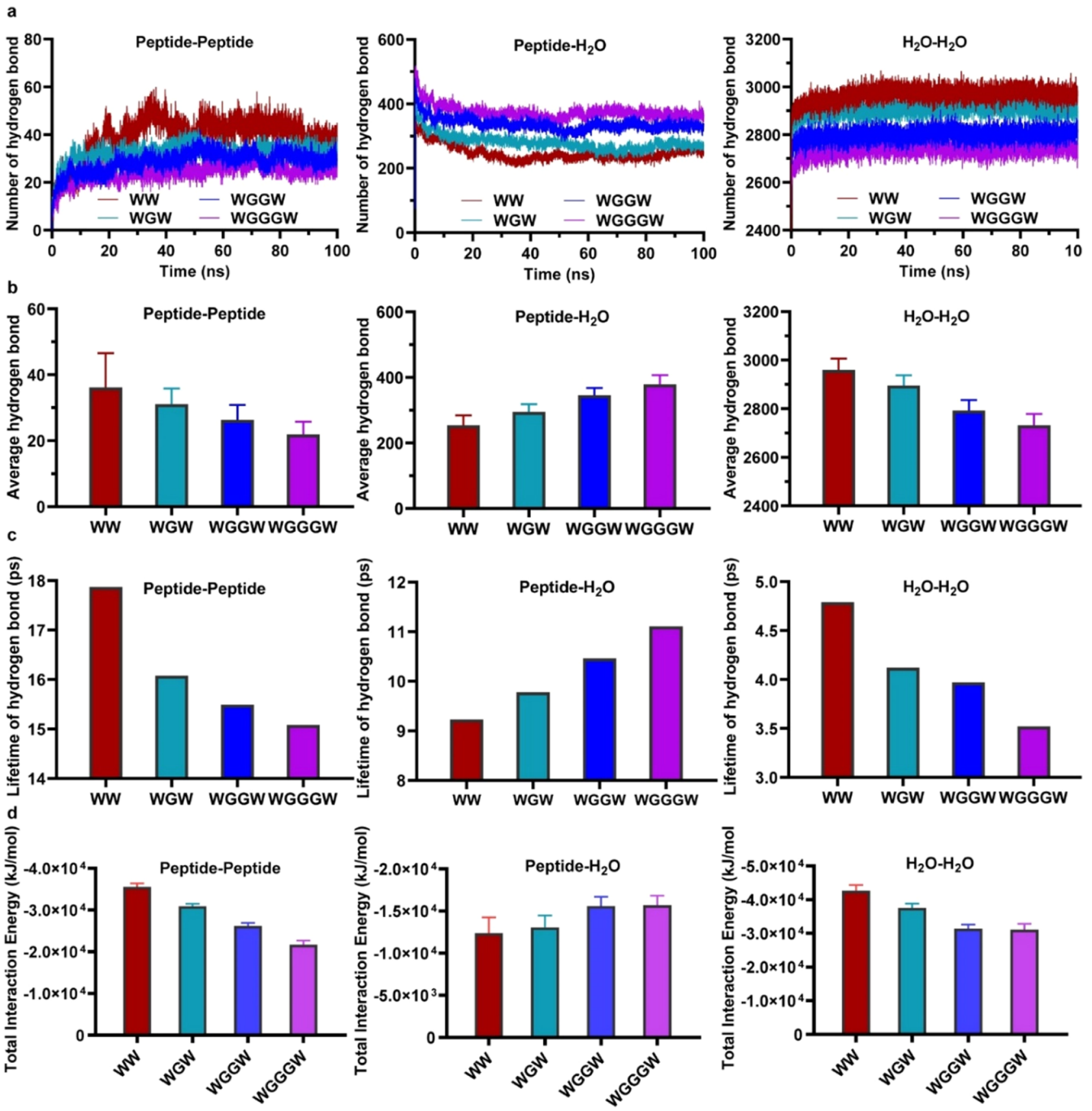

Figure 5. All-atom molecular dynamics (MD) simulation for the interaction between peptide−peptide, peptide-water, and water−water molecules. (a) Time-dependent number of hydrogen bonds between peptide−peptide, peptide-water, and water−water. (b) Calculated average of the hydrogen bond between peptide−peptide, peptide-water, and water−water. (c) Average lifetime of hydrogen bond between peptide−peptide, peptide-water, and water−water. (d) Total interaction energy between peptide−peptide, peptide-water, and water−water.

compact cluster, while in the WGGGW system, this increased to three clusters (Figure S1), implying a progressive enhancement in peptide−peptide interactions accompanied by a corresponding diminution in peptide-water interactions from the WW to the WGGGW system.

Subsequently, we calculated and compared the average number and lifetime of hydrogen bonds between peptide−peptide, peptide-water, and water−water interactions throughout the entire simulation duration. Both the number and lifetime of hydrogen bonds between peptides progressive decline from the WW to the WGGGW system (Figure 5a−c), revealing a diminishing strength in hydrogen bonding strength among the peptide molecules. Similar trends were observed for water−water interactions, while the peptide-water interactions demonstrated the opposite behavior (Figure 5a−c).

We also compared the changes in the $\pi-\pi$ stacking interactions across each system (Figure S2). The progressive reduction in $\pi-\pi$ stacking from WW to WGGGW corresponds with our previous observations that more robust $\pi-\pi$ interactions facilitate the formation of core−shell structures.[38,60] Finally, we systematically analyzed the total interaction energies of nonbonded interactions (including

https://doi.org/10.1021/jacs.5c10784
J. Am. Chem. Soc. XXXX, XXX, XXX−XXX

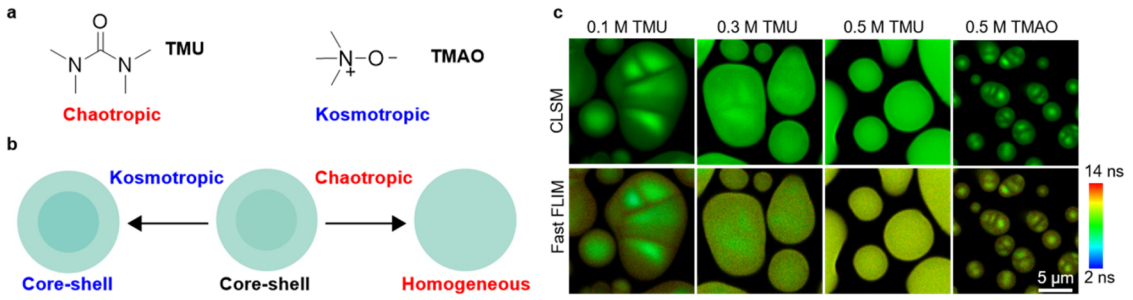

Figure 6. Dynamic regulation of the microstructure of condensates by "Chaotropic" and "Kosmotropic" agents. (a) Molecular structure of TMU and TMAO. (b) Schematic illustration of the influence of "Chaotropic" agent (TMU) and "Kosmotropic" agent (TMAO) on the microstructure of the condensates. (c) Microstructure changes of condensates formed by WGGW (10 mg/mL, pH 7.5 ± 0.5) with the treatment of different amounts of TMU and TMAO, respectively.

hydrogen bonds, electrostatic interactions, dispersion forces, $\pi-\pi$ stacking, and other noncovalent interactions) between peptide−peptide, peptide-water, and water−water across all four systems (Figure 5d). The results clearly demonstrate that peptide-water interactions intensified, while peptide−peptide and water−water interactions diminished progressively from the WW to the WGGGW system. All simulation results align consistently with our experimental data, further substantiating the notion that stronger peptide−peptide interactions facilitate the formation of core−shell droplets, whereas enhanced peptide-water interactions promote the development of homogeneous droplets.

Dynamically Regulation of Condensate Microstructure. We established the pivotal role of hydration water in shaping the microstructure of LLPS condensates. Our findings suggest that the transformation between core−shell condensates and homogeneous droplets can be modulated by adjusting the peptide-water interactions. To test this hypothesis, we employed "Chaotropic" and "Kosmotropic" agents—substances that disrupt or enhance the structure of water,[26] respectively. In our study, we selected the chaotropic agent tetramethylurea (TMU) and the kosmotropic agent trimethylamine N-oxide (TMAO). These agents have been extensively investigated in protein systems and model amide compounds, such as *N*-methylacetamide (NMA) systems.[61,62] TMU distorts the tetrahedral structure of water, thereby strengthening the interactions between the amide carbonyl group and water molecules. Conversely, TMAO enhances the tetrahedral structure of water, weakening the hydration of the carbonyl group. Essentially, TMU increases peptide-water interactions, while TMAO decreases them (Figure 6a). Fluorescence microscopy and FLIM revealed that heterogeneous condensates progressively transformed into homogeneous droplets with increasing concentrations of TMU. In contrast, the addition of TMAO accentuated the heterogeneous structure (Figure 6b,c). These findings not only underscore the significance of hydration water in regulating the substructure of LLPS condensates but also demonstrate that dynamic control over the transition between heterogeneous condensates and homogeneous droplets can be achieved by fine-tuning the balance between peptide−peptide and peptide-water interactions.

CONCLUSIONS

In summary, we engineered single-component short peptide droplets, presenting a novel strategy to modulate condensate structures from symmetric core−shell formations to homogeneous liquid droplets through the hydration effects of water. Our findings demonstrate that stronger peptide−peptide interactions promote the formation of core−shell condensates, while enhanced peptide-water interactions facilitate the emergence of homogeneous droplets. Utilizing molecular engineering, Fourier transform infrared spectroscopy, in situ Raman spectroscopy, and molecular dynamics simulations, we reveal that peptide-water interactions increase from WW to WGGGW. This shift leads to the transition of the inner core from a solid-like to a liquid-like state, enabling the transformation of core−shell condensates into homogeneous droplets. Furthermore, we established that droplet structures can be designed by modulating the hydrophilic and hydrophobic characteristics of the amino acid compositions.

Importantly, we demonstrated that the substructures of these condensates can be dynamically tuned using chaotropic and kosmotropic agents to adjust peptide-water interactions. Our work provides critical insights into the role of hydration water in LLPS, particularly regarding the liquid-to-solid transition processes in disease-related biomolecular condensates. The ability to rationally design core−shell peptide condensates offers a versatile platform for biomedical applications, particularly in targeted drug delivery. Surface functionalization of the outer shell enables selective cell targeting, while the core can serve as a reservoir for therapeutic agents, allowing for controlled and localized release. These features may help overcome major challenges in existing drug delivery systems, including limited targeting precision and suboptimal release kinetics. These findings open new avenues for designing and modulating the microstructure and functionality of advanced hydrated materials.

ASSOCIATED CONTENT

Supporting Information

The Supporting Information is available free of charge at https://pubs.acs.org/doi/10.1021/jacs.5c10784.

Experimental procedures and additional characterization, including details of peptide synthesis and characterization, NMR spectra and MD simulation (PDF)

AUTHOR INFORMATION

Corresponding Author

Huaimin Wang − *Department of Chemistry, Westlake University, Hangzhou 310030 Zhejiang, China;* orcid.org/0000-0002-8796-0367; Email: wanghuaimin@westlake.edu.cn

https://doi.org/10.1021/jacs.5c10784
J. Am. Chem. Soc. XXXX, XXX, XXX−XXX

Authors

Laicheng Zhou − *Department of Chemistry, Westlake University, Hangzhou 310030 Zhejiang, China*

Liheng Lu − *Department of Chemistry, Westlake University, Hangzhou 310030 Zhejiang, China*

Yang Zhang − *Department of Chemistry, Westlake University, Hangzhou 310030 Zhejiang, China*

Jing Wang − *Department of Chemistry, Westlake University, Hangzhou 310030 Zhejiang, China*

Jianjun Cheng − *School of Engineering, Westlake University, Hangzhou 310024 Zhejiang, China;* orcid.org/0000-0003-2561-9291

Complete contact information is available at: https://pubs.acs.org/10.1021/jacs.5c10784

Author Contributions

The manuscript was written through contributions of all authors. All authors have given approval to the final version of the manuscript.

Notes

The authors declare no competing financial interest.

■ ACKNOWLEDGMENTS

This project was supported by the National Natural Science Foundation of China (U24A2076, 82272145) and the Foundation of Westlake University. We thank the Instrumentation and Service Center for Molecular Sciences, Instrumentation and Service Center for Physical Sciences, General Equipment Core Facility, and Biomedical Research Core Facilities. We acknowledge Lingyu Xiao and Longchen Zhu for help with the fast FLIM experiments and discussion.

■ REFERENCES

(1) Ball, P. Water as an Active Constituent in Cell Biology. *Chem. Rev.* **2008**, *108* (1), 74−108.

(2) Pal, S. K.; Zewail, A. H. Dynamics of Water in Biological Recognition. *Chem. Rev.* **2004**, *104* (4), 2099−2124.

(3) Chaplin, M. Do we underestimate the importance of water in cell biology? *Nat. Rev. Mol. Cell Biol.* **2006**, *7* (11), 861−866.

(4) Bellissent-Funel, M.-C.; Hassanali, A.; Havenith, M.; Henchman, R.; Pohl, P.; Sterpone, F.; van der Spoel, D.; Xu, Y.; Garcia, A. E. Water Determines the Structure and Dynamics of Proteins. *Chem. Rev.* **2016**, *116* (13), 7673−7697.

(5) Levy, Y.; Onuchic, J. N. Water Mediation in Protein Folding and Molecular Recognition. *Annu. Rev. Biophys. Biomol. Struct.* **2006**, *35* (1), 389−415.

(6) Dong, S.; Leng, J.; Feng, Y.; Liu, M.; Stackhouse, C. J.; Schönhals, A.; Chiappisi, L.; Gao, L.; Chen, W.; Shang, J.; Jin, L.; Qi, Z.; Schalley, C. A. Structural water as an essential comonomer in supramolecular polymerization. *Sci. Adv.* **2017**, *3* (11), No. eaao0900.

(7) Zhao, Q.; Lee, D. W.; Ahn, B. K.; Seo, S.; Kaufman, Y.; Israelachvili, J. N.; Waite, J. H. Underwater contact adhesion and microarchitecture in polyelectrolyte complexes actuated by solvent exchange. *Nat. Mater.* **2016**, *15* (4), 407−412.

(8) Lee, H.; Lee, B. P.; Messersmith, P. B. A reversible wet/dry adhesive inspired by mussels and geckos. *Nature* **2007**, *448* (7151), 338−341.

(9) Finkelstein-Zuta, G.; Arnon, Z. A.; Vijayakanth, T.; Messer, O.; Lusky, O. S.; Wagner, A.; Zilberman, G.; Aizen, R.; Michaeli, L.; Rencus-Lazar, S.; Gilead, S.; Shankar, S.; Pavan, M. J.; Goldstein, D. A.; Kutchinsky, S.; Ellenbogen, T.; Palmer, B. A.; Goldbourt, A.; Sokol, M.; Gazit, E. A self-healing multispectral transparent adhesive peptide glass. *Nature* **2024**, *630* (8016), 368−374.

(10) Xing, P.; Li, Y.; Wang, Y.; Li, P. Z.; Chen, H.; Phua, S. Z. F.; Zhao, Y. Water-Binding-Mediated Gelation/Crystallization and Thermosensitive Superchirality. *Angew. Chem., Int. Ed.* **2018**, *57* (26), 7774−7779.

(11) Qin, C.; Ma, Y.; Zhang, Z.; Du, Y.; Duan, S.; Ma, S.; Pei, X.; Yu, B.; Cai, M.; He, X.; Zhou, F. Water-assisted strong underwater adhesion via interfacial water removal and self-adaptive gelation. *Proc. Natl. Acad. Sci. U.S.A.* **2023**, *120* (31), No. e2301364120.

(12) Vidyasagar, A.; Sureshan, K. M. Stoichiometric Sensing to Opt between Gelation and Crystallization. *Angew. Chem., Int. Ed.* **2015**, *54* (41), 12078−12082.

(13) Zhang, D.; Liu, J.; Chen, Q.; Jiang, W.; Wang, Y.; Xie, J.; Ma, K.; Shi, C.; Zhang, H.; Chen, M.; Wan, J.; Ma, P.; Zou, J.; Zhang, W.; Zhou, F.; Liu, R. A sandcastle worm-inspired strategy to functionalize wet hydrogels. *Nat. Commun.* **2021**, *12* (1), No. 6331.

(14) Arya, S.; Singh, A. K.; Khan, T.; Bhattacharya, M.; Datta, A.; Mukhopadhyay, S. Water Rearrangements upon Disorder-to-Order Amyloid Transition. *J. Phys. Chem. Lett.* **2016**, *7* (20), 4105−4110.

(15) Thirumalai, D.; Reddy, G.; Straub, J. E. Role of Water in Protein Aggregation and Amyloid Polymorphism. *Acc. Chem. Res.* **2012**, *45* (1), 83−92.

(16) Fichou, Y.; Schirò, G.; Gallat, F.-X.; Laguri, C.; Moulin, M.; Combet, J.; Zamponi, M.; Härtlein, M.; Picart, C.; Mossou, E.; Lortat-Jacob, H.; Colletier, J.-P.; Tobias, D. J.; Weik, M. Hydration water mobility is enhanced around tau amyloid fibers. *Proc. Natl. Acad. Sci. U.S.A.* **2015**, *112* (20), 6365−6370.

(17) Ortony, J. H.; Qiao, B.; Newcomb, C. J.; Keller, T. J.; Palmer, L. C.; Deiss-Yehiely, E.; de la Cruz, M. O.; Han, S.; Stupp, S. I. Water Dynamics from the Surface to the Interior of a Supramolecular Nanostructure. *J. Am. Chem. Soc.* **2017**, *139* (26), 8915−8921.

(18) Dey, A.; Naranjo, E.; Saha, R.; Zhang, S.; Nair, M. N.; Li, T.-D.; Chen, X.; Ulijn, R. V. Water-Vapor Responsive Metallo-Peptide Nanofibers. *Angew. Chem., Int. Ed.* **2024**, *63* (47), No. e202409391.

(19) Huang, Z.; Kang, S.-K.; Banno, M.; Yamaguchi, T.; Lee, D.; Seok, C.; Yashima, E.; Lee, M. Pulsating Tubules from Noncovalent Macrocycles. *Science* **2012**, *337* (6101), 1521−1526.

(20) Arazoe, H.; Miyajima, D.; Akaike, K.; Araoka, F.; Sato, E.; Hikima, T.; Kawamoto, M.; Aida, T. An autonomous actuator driven by fluctuations in ambient humidity. *Nat. Mater.* **2016**, *15* (10), 1084−1089.

(21) Ma, M.; Guo, L.; Anderson, D. G.; Langer, R. Bio-inspired polymer composite actuator and generator driven by water gradients. *Science* **2013**, *339* (6116), 186−189.

(22) Gianti, E.; Delemotte, L.; Klein, M. L.; Carnevale, V. On the role of water density fluctuations in the inhibition of a proton channel. *Proc. Natl. Acad. Sci. U.S.A.* **2016**, *113* (52), E8359−E8368.

(23) Fu, H.; Huang, J.; van der Tol, J. J.; Su, L.; Wang, Y.; Dey, S.; Zijlstra, P.; Fytas, G.; Vantomme, G.; Dankers, P. Y.; Meijer, E. W. Supramolecular polymers form tactoids through liquid−liquid phase separation. *Nature* **2024**, *626* (8001), 1011−1018.

(24) Su, L.; Mosquera, J.; Mabesoone, M. F.; Schoenmakers, S. M.; Muller, C.; Vleugels, M. E.; Dhiman, S.; Wijker, S.; Palmans, A. R.; Meijer, E. Dilution-induced gel-sol-gel-sol transitions by competitive supramolecular pathways in water. *Science* **2022**, *377* (6602), 213−218.

(25) Duijs, H.; Kumar, M.; Dhiman, S.; Su, L. Harnessing competitive interactions to regulate supramolecular "micelle-droplet-fiber" transition and reversibility in water. *J. Am. Chem. Soc.* **2024**, *146* (43), 29759−29766.

(26) Brini, E.; Fennell, C. J.; Fernandez-Serra, M.; Hribar-Lee, B.; Lukšič, M.; Dill, K. A. How Water's Properties Are Encoded in Its Molecular Structure and Energies. *Chem. Rev.* **2017**, *117* (19), 12385−12414.

(27) Ribeiro, S. S.; Samanta, N.; Ebbinghaus, S.; Marcos, J. C. The synergic effect of water and biomolecules in intracellular phase separation. *Nat. Rev. Chem.* **2019**, *3* (9), 552−561.

(28) Brangwynne, C. P.; Tompa, P.; Pappu, R. V. Polymer physics of intracellular phase transitions. *Nat. Phys.* **2015**, *11* (11), 899−904.

(29) Pappu, R. V.; Cohen, S. R.; Dar, F.; Farag, M.; Kar, M. Phase Transitions of Associative Biomacromolecules. *Chem. Rev.* **2023**, *123* (14), 8945−8987.

(30) Zaslavsky, B. Y.; Uversky, V. N. In Aqua Veritas: The Indispensable yet Mostly Ignored Role of Water in Phase Separation and Membrane-less Organelles. *Biochemistry* **2018**, *57* (17), 2437−2451.
(31) Zaslavsky, B. Y.; Bagirov, T. O.; Borovskaya, A. A.; Gulaeva, N. D.; Miheeva, L. H.; Mahmudov, A. U.; Rodnikova, M. N. Structure of water as a key factor of phase separation in aqueous mixtures of two nonionic polymers. *Polymer* **1989**, *30* (11), 2104−2111.
(32) Ahlers, J.; Adams, E. M.; Bader, V.; Pezzotti, S.; Winklhofer, K. F.; Tatzelt, J.; Havenith, M. The key role of solvent in condensation: Mapping water in liquid-liquid phase-separated FUS. *Biophys. J.* **2021**, *120* (7), 1266−1275.
(33) Mukherjee, S.; Schäfer, L. V. Thermodynamic forces from protein and water govern condensate formation of an intrinsically disordered protein domain. *Nat. Commun.* **2023**, *14* (1), No. 5892.
(34) Joshi, A.; Avni, A.; Walimbe, A.; Rai, S. K.; Sarkar, S.; Mukhopadhyay, S. Hydrogen-Bonded Network of Water in Phase-Separated Biomolecular Condensates. *J. Phys. Chem. Lett.* **2024**, *15* (30), 7724−7734.
(35) Pezzotti, S.; König, B.; Ramos, S.; Schwaab, G.; Havenith, M. Liquid−Liquid Phase Separation? Ask the Water! *J. Phys. Chem. Lett.* **2023**, *14* (6), 1556−1563.
(36) Abbas, M.; Lipiński, W. P.; Nakashima, K. K.; Huck, W. T. S.; Spruijt, E. A short peptide synthon for liquid-liquid phase separation. *Nat. Chem.* **2021**, *13* (11), 1046−1054.
(37) Tang, Y.; Bera, S.; Yao, Y.; Zeng, J.; Lao, Z.; Dong, X.; Gazit, E.; Wei, G. Prediction and characterization of liquid-liquid phase separation of minimalistic peptides. *Cell Rep. Phys. Sci.* **2021**, *2* (9), No. 100579.
(38) Zhou, L.; Zhu, L.; Wang, C.; Xu, T.; Wang, J.; Zhang, B.; Zhang, X.; Wang, H. Multiphasic condensates formed with mono-component of tetrapeptides via phase separation. *Nat. Commun.* **2025**, *16* (1), No. 2706.
(39) Baruch Leshem, A.; Sloan-Dennison, S.; Massarano, T.; Ben-David, S.; Graham, D.; Faulds, K.; Gottlieb, H. E.; Chill, J. H.; Lampel, A. Biomolecular condensates formed by designer minimalistic peptides. *Nat. Commun.* **2023**, *14* (1), No. 421.
(40) Takeuchi, H. Raman structural markers of tryptophan and histidine side chains in proteins. *Biopolymers* **2003**, *72* (5), 305−317.
(41) Guo, Q.; Zou, G.; Qian, X.; Chen, S.; Gao, H.; Yu, J. Hydrogen-bonds mediate liquid-liquid phase separation of mussel derived adhesive peptides. *Nat. Commun.* **2022**, *13* (1), No. 5771.
(42) Rekhi, S.; Garcia, C. G.; Barai, M.; Rizuan, A.; Schuster, B. S.; Kiick, K. L.; Mittal, J. Expanding the molecular language of protein liquid−liquid phase separation. *Nat. Chem.* **2024**, *16* (7), 1113−1124.
(43) Ganar, K. A.; Nandy, M.; Turbina, P.; Chen, C.; Suylen, D.; Nihoul, E.; Pascoe, E. L.; van der Beelen, S.; Plaum, M.; van den Bos, L.; Koenraadt, C. J. M.; Dijkgraaf, I.; Deshpande, S. Phase separation and ageing of glycine-rich protein from tick adhesive. *Nat. Chem.* **2025**, *17* (2), 186−197.
(44) Ye, S.; Latham, A. P.; Tang, Y.; Hsiung, C. H.; Chen, J.; Luo, F.; Liu, Y.; Zhang, B.; Zhang, X. Micropolarity governs the structural organization of biomolecular condensates. *Nat. Chem. Biol.* **2024**, *20* (4), 443−451.
(45) Ghosh, A.; Zhou, H. X. Determinants for Fusion Speed of Biomolecular Droplets. *Angew. Chem., Int. Ed.* **2020**, *59* (47), 20837−20840.
(46) Jawerth, L.; Fischer-Friedrich, E.; Saha, S.; Wang, J.; Franzmann, T.; Zhang, X.; Sachweh, J.; Ruer, M.; Ijavi, M.; Saha, S.; Mahamid, J.; Hyman, A. A.; Jülicher, F. Protein condensates as aging Maxwell fluids. *Science* **2020**, *370* (6522), 1317−1323.
(47) Pullanchery, S.; Kulik, S.; Rehl, B.; Hassanali, A.; Roke, S. Charge transfer across C−H···O hydrogen bonds stabilizes oil droplets in water. *Science* **2021**, *374* (6573), 1366−1370.
(48) Wang, Y.-H.; Zheng, S.; Yang, W.-M.; Zhou, R.-Y.; He, Q.-F.; Radjenovic, P.; Dong, J.-C.; Li, S.; Zheng, J.; Yang, Z.-L.; Attard, G.; Pan, F.; Tian, Z.-Q.; Li, J.-F. In situ Raman spectroscopy reveals the structure and dissociation of interfacial water. *Nature* **2021**, *600* (7887), 81−85.
(49) Heilweil, E. J. Ultrafast Glimpses at Water and Ice. *Science* **1999**, *283* (5407), 1467−1468.
(50) Yu, C.-C.; Chiang, K.-Y.; Okuno, M.; Seki, T.; Ohto, T.; Yu, X.; Korepanov, V.; Hamaguchi, H.-o.; Bonn, M.; Hunger, J.; Nagata, Y. Vibrational couplings and energy transfer pathways of water's bending mode. *Nat. Commun.* **2020**, *11* (1), No. 5977.
(51) Davis, J. G.; Gierszal, K. P.; Wang, P.; Ben-Amotz, D. Water structural transformation at molecular hydrophobic interfaces. *Nature* **2012**, *491* (7425), 582−585.
(52) Seo, J.; Hoffmann, W.; Warnke, S.; Huang, X.; Gewinner, S.; Schöllkopf, W.; Bowers, M. T.; von Helden, G.; Pagel, K. An infrared spectroscopy approach to follow β-sheet formation in peptide amyloid assemblies. *Nat. Chem.* **2017**, *9* (1), 39−44.
(53) Barth, A. Infrared spectroscopy of proteins. *Biochim. Biophys. Acta, Bioenerg.* **2007**, *1767* (9), 1073−1101.
(54) Van Der Spoel, D.; Lindahl, E.; Hess, B.; Groenhof, G.; Mark, A. E.; Berendsen, H. J. C. GROMACS: Fast, flexible, and free. *J. Comput. Chem.* **2005**, *26* (16), 1701−1718.
(55) Jorgensen, W. L.; Chandrasekhar, J.; Madura, J. D.; Impey, R. W.; Klein, M. L. Comparison of simple potential functions for simulating liquid water. *J. Chem. Phys.* **1983**, *79* (2), 926−935.
(56) Darden, T.; York, D.; Pedersen, L. Particle mesh Ewald: An N·log(N) method for Ewald sums in large systems. *J. Chem. Phys.* **1993**, *98* (12), 10089−10092.
(57) Hess, B.; Bekker, H.; Berendsen, H. J. C.; Fraaije, J. G. E. M. LINCS: A linear constraint solver for molecular simulations. *J. Comput. Chem.* **1997**, *18* (12), 1463−1472.
(58) Berendsen, H. J. C.; Postma, J. P. M.; van Gunsteren, W. F.; DiNola, A.; Haak, J. R. Molecular dynamics with coupling to an external bath. *J. Chem. Phys.* **1984**, *81* (8), 3684−3690.
(59) Martoňák, R.; Laio, A.; Parrinello, M. Predicting Crystal Structures: The Parrinello-Rahman Method Revisited. *Phys. Rev. Lett.* **2003**, *90* (7), No. 075503.
(60) Li, J.; Du, X.; Hashim, S.; Shy, A.; Xu, B. Aromatic−Aromatic Interactions Enable α-Helix to β-Sheet Transition of Peptides to Form Supramolecular Hydrogels. *J. Am. Chem. Soc.* **2017**, *139* (1), 71−74.
(61) Wei, H.; Fan, Y.; Gao, Y. Q. Effects of Urea, Tetramethyl Urea, and Trimethylamine N-Oxide on Aqueous Solution Structure and Solvation of Protein Backbones: A Molecular Dynamics Simulation Study. *J. Phys. Chem. B* **2010**, *114* (1), 557−568.
(62) Bolen, D. W.; Rose, G. D. Structure and Energetics of the Hydrogen-Bonded Backbone in Protein Folding. *Annu. Rev. Biochem.* **2008**, *77* (1), 339−362.

https://doi.org/10.1021/jacs.5c10784
J. Am. Chem. Soc. XXXX, XXX, XXX−XXX